Phase diagram and electrochemical properties of mixed olivines from first-principles calculations

Rahul Malik,[1] Fei Zhou (周非),[2] and Gerbrand Ceder[1]
[1]*Department of Materials Science and Engineering, Massachusetts Institute of Technology, 77 Massachusetts Avenue, Cambridge, Massachusetts 02139, USA*
[2]*Department of Materials Science and Engineering, University of California, Los Angeles, California 90095, USA*
(Received 7 April 2009; revised manuscript received 15 May 2009; published 4 June 2009)

Using first-principles calculations, we study the effect of cation substitution on the transition-metal sublattice in phospho-olivines, with special attention given to the $Li_x(Fe_{1-y}Mn_y)PO_4$ system. We use a cluster expansion model derived from first-principles with Monte Carlo simulations to calculate finite-T phase diagrams, voltage curves, and solubility limits of the system. The phase diagram of $Li_x(Fe_{1-y}Mn_y)PO_4$ shows two low-temperature miscibility gaps separated by a solid solution phase centered at Li composition $x \approx y$, which corresponds to a state where most Fe ions are oxidized and most Mn are not. This intermediate low-T solid solution is stabilized by the dilution of phase-separating interactions caused by the disorder of redox potentials on the transition-metal sites. The calculated voltage curves show two plateaus at ~4–4.2 V and ~3.5–3.7 V, corresponding to the Mn^{3+}/Mn^{2+} and Fe^{3+}/Fe^{2+} redox couples, respectively, with an extended sloping region in between corresponding to the low-T solid solution phase. In agreement with experiment, we find that the Mn^{3+}/Mn^{2+} (Fe^{3+}/Fe^{2+}) voltage is decreased (increased) by Fe (Mn) substitution. We explain this by considering the energy of the solid solution which is the discharged (charged) state for these redox couples and argue that such changes are generic to all mixed olivine systems. We also find reduced phase transformation polarization on both plateaus which we attribute to the decreased composition difference between the oxidized and reduced state for each redox couple

DOI: 10.1103/PhysRevB.79.214201 PACS number(s): 82.47.Aa

I. INTRODUCTION

With the emergence of $LiFePO_4$ as a viable battery cathode material for large format batteries, cation-substituted phospho-olivine systems of the form $Li(Fe_{1-y}M_y)PO_4$ (M =Mn or Co) have gained the interest of battery researchers.[1–15] Specifically, the prospect of improved energy density over $LiFePO_4$ due to the higher redox potential of Mn^{3+}/Mn^{2+} compared to Fe^{3+}/Fe^{2+} [~4.1 V compared to ~3.4 V vs Li/Li^+ (Ref. 16)] has fuelled research into $Li(Fe_{1-y}Mn_y)PO_4$.[1,3,5–7,11] Several questions in particular arise for mixed cation systems: $LiFePO_4$ is delithiated in a two-phase reaction forming $FePO_4$, and both phases tolerate only a small amount of off-stoichiometry.[17] Zhou *et al.* showed that this two-phase reaction is unusual and driven by the strong electron-Li^+ interaction.[18] Dilution of the Fe sites by Mn may modify the phase behavior upon delithiation. In particular, Yamada *et al.* observed that the reduction of Fe^{3+} to Fe^{2+} shifts from two-phase to single-phase upon Li insertion for samples with $0.2 \leq y \leq 0.6$ (samples with y=0, 0.2, 0.4, 0.6, 0.8, and 1.0 were tested, but those with $y \geq 0.8$ were unstable and did not completely retain the olivine structure in the delithiated state) while the Mn reaction remains entirely two-phase for $y \leq 0.8$.[1]

Our approach is to use first-principles calculation to study the temperature-composition phase diagram of $Li_x(Fe_{1-y}Mn_y)PO_4$ for different Mn-Fe compositions. In the case of $LiFePO_4$, both first-principles investigations and experiments have helped explain the observed low-temperature phase separation,[18–20] diffusion path of Li,[21–23] and high-rate capability.[24] Of particular interest, first-principles calculations by Zhou *et al.*[18] which take into account both lithium/vacancy (Li^+/V) and electron/hole (e^-/h^+) configurational entropy have proven accurate in predicting the finite-T phase behavior of the Li_xFePO_4 system. In this work, a modification to that model has been incorporated to take into account Mn substitution of Fe. The resulting phase diagram of $Li_x(Fe_{1-y}Mn_y)PO_4$, voltage curves, and solubility limits are reported and compared to experiment. We also study the change in polarization and hysteresis associated with the first-order phase transition as Mn is substituted for Fe.

II. METHODS

The model used in this work builds on the approach proposed by Zhou *et al.*[18] which was used to determine the phase diagram of Li_xFePO_4. In that work, a coupled cluster expansion taking into account both ionic and electronic degrees of freedom was parametrized from generalized gradient approximation + U (GGA+U) *ab initio* calculations[16] and then used as a Hamiltonian in Monte Carlo (MC) simulations. By thermalizing both the Li^+/V and e^-/h^+ distributions, the free energy can be obtained for any temperature and Li concentration. In essence, a cluster expansion is a representation of the energy of the system in the phase space of all Li^+/V and e^-/h^+ distributions. The typical form of the energy model is a polynomial expansion in the occupation variables at each site,

$$E[\vec{\lambda},\vec{\varepsilon}] = J_o + J_i\lambda_i + J_{ij}\lambda_i\lambda_j + J_{ia}\lambda_i\varepsilon_a + J_{ab}\varepsilon_a\varepsilon_b + \cdots . \quad (1)$$

In Eq. (1), λ_i represents occupancy of Li^+ site i, where λ_i =1 represents Li^+ occupation and λ_i=−1 represents vacancy occupation. Similarly, ε_a represents occupancy of iron site a, where ε_a=1 represents electron (Fe^{2+}) occupation and ε_a= −1 represents hole (Fe^{3+}) occupation. The J coefficients are

the effective cluster interactions (ECIs), which reflect the aggregate effect of several physical factors such as electrostatics, screening, relaxation, covalency, etc. Because the Fe^{3+}/Fe^{2+} sublattice and the Li^{+}/V sublattice do not coincide, this is a coupled cluster expansion rather than a quaternary model.[25]

In this work, the same cluster expansion by Zhou *et al.*[18] was used, apart from one modification. In order to simulate the $Li_x(Fe_{1-y}Mn_y)PO_4$ system, we replace the transition-metal point term by

$$\Delta E = \sum_{a \in \text{Mn Sites}} J_{\text{Mn}} \varepsilon_a + \sum_{a \in \text{Fe Sites}} J_{\text{Fe}} \varepsilon_a, \qquad (2)$$

where $J_{\text{Mn}} = -4.2$ eV/2 and $J_{\text{Fe}} = -3.5$ eV/2. This represents the electron energy on the transition-metal site shifted down by 0.7 eV/2 on a fixed set of randomly chosen metal sites to account for Mn substitution. The factor of 1/2 is due to the fact that in our formulation, the redox reaction of hole to electron state is represented by the change in occupation variable ε_a from −1 to 1. It is well documented in both experiments and first-principles calculations that the difference between redox voltages of $LiMnPO_4$ and $LiFePO_4$ with respect to Li is ~0.7 V.[16,26,27] Since the point term ECI roughly corresponds to the chemical potential (i.e., the voltage), the model used in this work approximately takes into account the difference in redox potential associated with Mn versus Fe. Since in our model Mn only modifies the interactions in Li_xFePO_4 by the e^-/h^+ site energy on the Mn position, higher-order Mn-specific interactions such as Jahn-Teller distortion are not taken into account. We will discuss the implications of this later.

Monte Carlo simulations were performed at different temperatures and degrees of Mn substitution in $6 \times 12 \times 12$ and $12 \times 12 \times 12$ supercells (50 000 MC steps and 10 000 equilibration steps), where one cell corresponds to four $Li_x(Fe_{1-y}Mn_y)PO_4$ formula units. The free energy at each composition was obtained by integrating the relation between μ_{Li} and x_{Li}.

III. RESULTS

To observe the effect of Mn on the voltage profile (Li content on x axis, voltage on y axis), Monte Carlo simulations were performed as a function of μ_{Li} at constant temperature for several Mn compositions. A typical calculated voltage profile output is shown in Fig. 1 for $y=0.6$, showing noticeable hysteresis between charge (decreasing μ_{Li}) and discharge (increasing μ_{Li}). Free-energy integration[28] is employed to obtain the equilibrium voltage profile and thus remove the hysteresis, the result of which is shown in Fig. 2 for several Mn compositions. The voltage curves show two plateaus at ~4–4.2 V and ~3.5–3.7 V, corresponding to the Mn^{3+}/Mn^{2+} and Fe^{3+}/Fe^{2+} redox couples, respectively. This can be readily seen since the widths of the plateaus (in Li composition) are roughly equal to the Mn/Fe compositions. The slight discrepancy of the calculated voltages as compared to experiments is typical for the GGA+U approximation to obtain energies.[16] Constant voltage (chemical-potential) regions correspond to first-order phase transitions

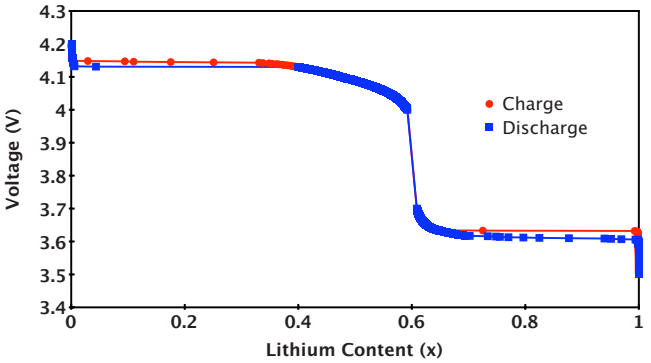

FIG. 1. (Color online) Calculated charge (red circles) and discharge (blue squares) voltage curve of $Li_x(Fe_{0.4}Mn_{0.6})PO_4$ at 300 K as determined by Monte Carlo ($12 \times 12 \times 12$ cell size) simulation.

and thus phase-separated regions in Li composition, and regions with varying voltage correspond to single-phase regions. Between the Mn^{3+}/Mn^{2+} and Fe^{3+}/Fe^{2+} plateaus is an extended single-phase region in which most Fe is oxidized while most Mn is not.

The information determined from the voltage curves shown in Fig. 2 can be summarized by plotting the composition at the phase boundaries as shown in Fig. 3 with Li content (x) along the x axis and Mn content (y) along the y axis. Region (a) is phase-separated corresponding to the Mn^{3+}/Mn^{2+} couple; region (b) is single-phase corresponding to Mn^{3+}/Mn^{2+} (shaded region) and Fe^{3+}/Fe^{2+} (unshaded region); and region (c) is phase-separated corresponding to Fe^{3+}/Fe^{2+}. The dashed line corresponds to the experimentally determined boundary between single-phase Fe^{3+}/Fe^{2+} and phase-separated Fe^{3+}/Fe^{2+} by Yamada *et al.*[1]

The results from free-energy integrations at different temperatures can be used to construct phase diagrams [lithium content (x) along the x axis and temperature along the y axis] as shown in Fig. 4. The phase diagram of Li_xFePO_4 ($0 \leq x \leq 1$), determined by both experiment[19,20] and first-principles calculations,[18] shows a low-temperature miscibility gap between $FePO_4$ and $LiFePO_4$ and a eutectoid transition to a solid solution (SS) phase. By substituting Mn on the Fe sublattice, the solid solution phase is stabilized at low tempera-

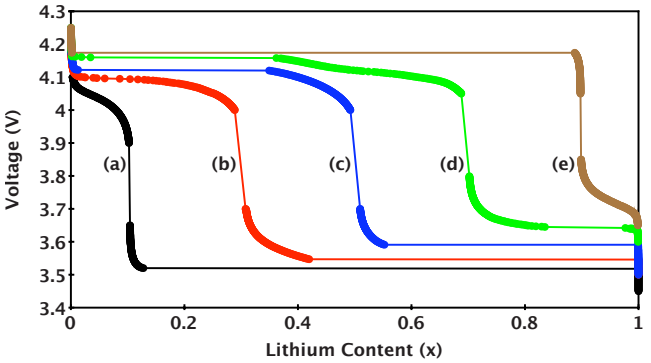

FIG. 2. (Color online) Equilibrium voltage curves of $Li_x(Fe_{1-y}Mn_y)PO_4$ at 300 K for (a) $y=0.1$, (b) $y=0.3$, (c) $y=0.5$, (d) $y=0.7$, and (e) $y=0.9$ as determined by Monte Carlo free-energy integration.

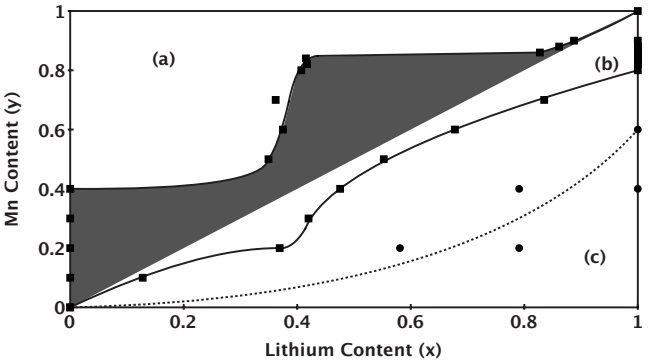

FIG. 3. Summary phase diagram of the $Li_x(Fe_{1-y}Mn_yPO_4)$ system at 300 K. Squares denote the boundaries between phase-separated and single-phase regions. Region (a) corresponds to a two-phase region associated with the Mn^{3+}/Mn^{2+} couple; Region (b) corresponds to a single-phase region associated with the Mn^{3+}/Mn^{2+} couple (shaded region) and the Fe^{3+}/Fe^{2+} couple (unshaded); Region (c) corresponds to a two-phase region associated with the Fe^{3+}/Fe^{2+} couple. Circles correspond to the boundary between the two-phase and single-phase regions associated with the Fe^{3+}/Fe^{2+} couple as determined experimentally by Yamada *et al.* (Ref. 1). The dashed line denotes the experimentally determined boundary between single-phase Fe^{3+}/Fe^{2+} and phase-separated Fe^{3+}/Fe^{2+} as determined by Yamada *et al.* (Ref. 1).

ture, and the phase diagram consists of two miscibility gaps at low temperature, the first between $Fe_{1-y}Mn_yPO_4$ (denoted α in Fig. 4) and $Li_yFe_{1-y}Mn_yPO_4$ (denoted SS in Fig. 4) and the second between $Li_yFe_{1-y}Mn_yPO_4$ (SS) and $LiFe_{1-y}Mn_yPO_4$ (denoted β in Fig. 4), where $0 \leq y \leq 1$. Several observations can be made from these results. First, the miscibility gap of the minority redox couple (e.g., Mn^{3+}/Mn^{2+} for $y<0.5$ or Fe^{3+}/Fe^{2+} for $y>0.5$) is lower in temperature than the miscibility gap of the majority redox couple. This can be understood from the fact that as a redox center is diluted in concentration, the effective interactions that create the miscibility gap are also diluted, thereby lowering the transition temperature to solid solution. Second, the solid solution phase penetrates between the two miscibility gaps down to low T at a Li composition that is approximately equal to the amount of Mn (y).

Figure 2 clearly shows that the voltage at which the phase transition occurs (hereafter referred to as the transition voltage) for both Fe^{3+}/Fe^{2+} and Mn^{3+}/Mn^{2+} couples increases as Mn content increases. The values of the transition voltage at 300 K for both couples as a function of Mn composition are cataloged in Fig. 5. The voltage for both redox couples steadily increases with Mn composition. It is also shown that the phase transition shifts from first order to second order with increasing Mn substitution for the Fe^{3+}/Fe^{2+} couple, and the opposite is seen for the Mn^{3+}/Mn^{2+} couple.

Figure 6 shows the voltage of the Fe^{3+}/Fe^{2+} first-order phase transition upon both charge and discharge in the Monte Carlo simulation at different degrees of Mn substitution and a comparison to the experiments performed by Nakamura *et al.*[10] on the $Li_xFe_{1-y}Mn_yPO_4$ system. Similarly, Fig. 7 shows the transition voltages upon charge and discharge of the Mn^{3+}/Mn^{2+} first-order phase transition with increasing Mn

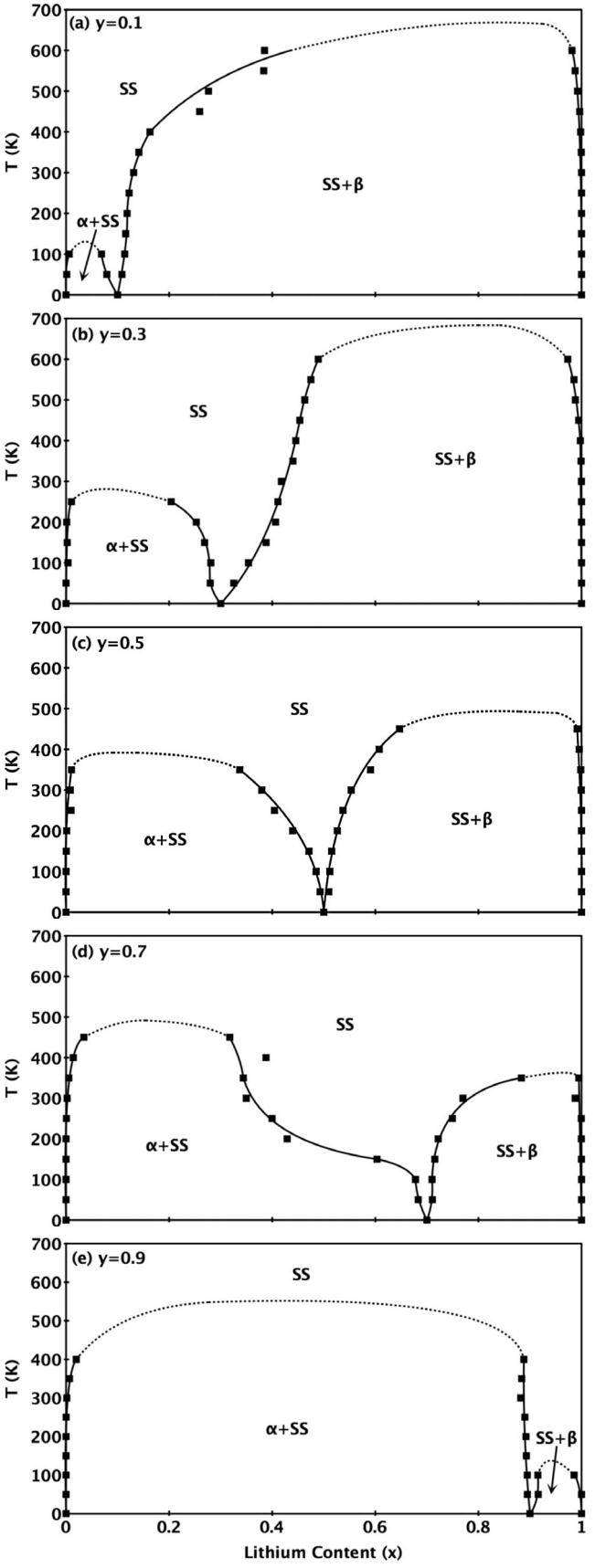

FIG. 4. Calculated phase diagrams of $Li_x(Fe_{1-y}Mn_y)PO_4$ for (a) $y=0.1$, (b) $y=0.3$, (c) $y=0.5$, (d) $y=0.7$, and (e) $y=0.9$. Dashed line is speculative.

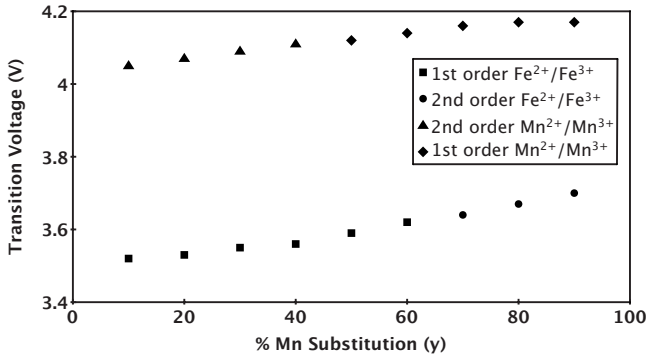

FIG. 5. Equilibrium phase-transition voltages at 300 K for Fe^{3+}/Fe^{2+} and Mn^{3+}/Mn^{2+}.

substitution. In both Figs. 6 and 7, the same trend of increasing transition voltage with Mn substitution is observed. Also, the difference between the transition voltage determined upon charge and discharge (as discussed earlier and shown as the hysteresis in Fig. 1) decreases with increasing Mn substitution for the Fe^{3+}/Fe^{2+} couple and increases for the Mn^{3+}/Mn^{2+} couple. This effect is shown clearly in Fig. 8, which shows the polarization, defined as the difference between the charge and discharge transition voltages, at different degrees of Mn substitution for both the Fe^{3+}/Fe^{2+} and Mn^{3+}/Mn^{2+} couples.

IV. DISCUSSION

Most of the trends we find compare well to the available experimental work. In experimentally determined charge-discharge curves and open-circuit voltage (OCV) measurements of the $Li_x(Fe_yMn_{1-y})PO_4$ system,[2,3,6,7] two plateaus at ~3.5 and ~4.1 V are observed with a sloping (single-phase) region in between connecting the two, which shows good qualitative agreement with the data presented in Fig. 2. Also, the experimentally obtained voltage curves show similar variation in the plateau width with increasing Mn composition as observed in Fig. 2.[2,3,6,7] The trends observed in Figs. 5–8, of increasing transition voltage and reduced polarization of the Fe^{3+}/Fe^{2+} transition with increasing Mn composition,

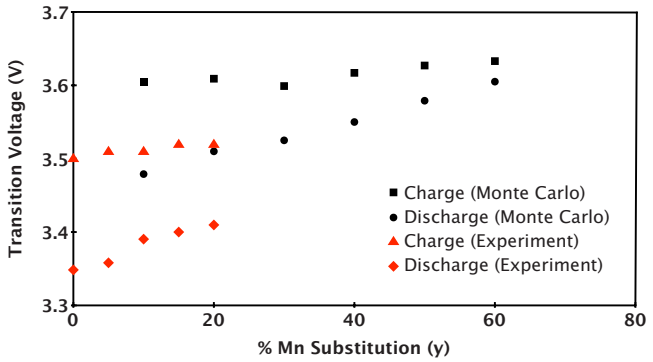

FIG. 6. (Color online) Phase-transition voltages of the Fe^{3+}/Fe^{2+} couple as determined by Monte Carlo ($12\times12\times12$ cell size) simulation upon charge and discharge compared to experiments by Nakamura *et al.* (Ref. 10).

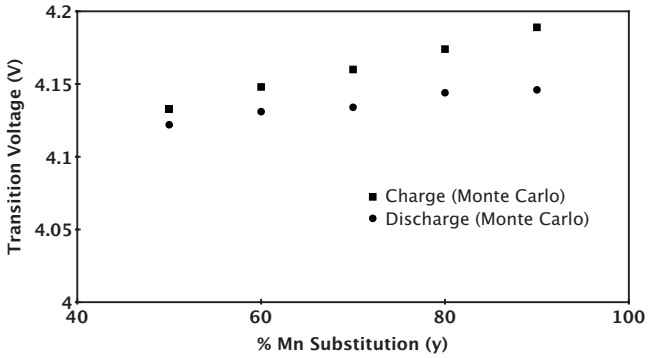

FIG. 7. First-order phase-transition voltages of the Mn^{3+}/Mn^{2+} couple as determined by Monte Carlo ($12\times12\times12$ cell size) simulation upon charge and discharge.

are similarly reflected in experimental data.[9,10,29] Experimental polarization and transition voltage data of the Mn^{3+}/Mn^{2+} transition is unavailable, but experimental data in the $Li_x(Fe_{1-y}Co_y)PO_4$ system[12] reflects a similar trend of increasing polarization and transition voltage of the Co^{3+}/Co^{2+} transition with increasing Co content. While this is a different system, it serves to illustrate how a higher redox couple is modified by the presence of the Fe^{3+}/Fe^{2+} couple.

Experiments performed by Yamada *et al.*[1] do not produce a single-phase Mn^{3+}/Mn^{2+} region when the Mn couple is diluted by Fe as we find in the shaded portion of Fig. 3. We believe that this difference between the calculations and experiments is due to the specific Jahn-Teller nature of Mn^{3+}. The Jahn-Teller distortion around Mn^{3+} leads to a large lattice distortion. Typically, when large elastic effects are present around impurities, solid solution regions are small, and a first-order phase is preferred because a collective distortion of the unit cell results in less elastic strain energy than the combined elastic distortions around single impurities. The model used in this work represents Mn only by modifying the point term in the coupled cluster expansion determined for the Li_xFePO_4 system, leaving all higher-order ECIs unchanged. Thus, Mn-specific higher-order interactions are neglected in the model. These findings support the widely held opinion that the underlying physics of the $LiMnPO_4$

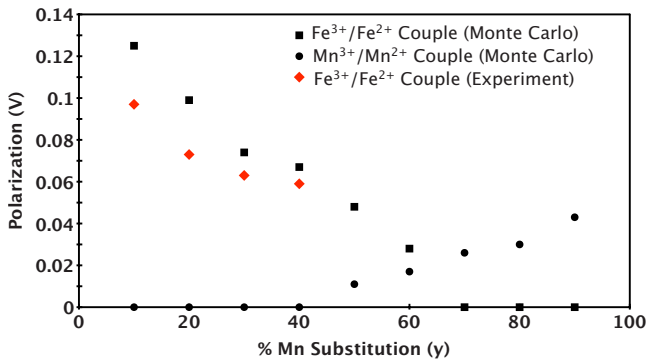

FIG. 8. (Color online) Polarization, defined as the difference between charge and discharge voltages, for Fe^{3+}/Fe^{2+} and Mn^{3+}/Mn^{2+} couples as determined by Monte Carlo ($12\times12\times12$ cell size) simulation compared to experiments by Nakamura *et al.* (Ref. 10).

system are different compared to the $LiFePO_4$ system.[1,30] Hence, while the phase diagram of the pure Li_xMnPO_4 system has not been investigated, it seems likely that the temperature at which solid solution occurs is higher than in Li_xFePO_4 due to the stronger phase-separation interaction caused by the Mn^{3+} Jahn-Teller distortion.

A. Existence of single-phase region

To understand the phase behavior in $Li_x(Fe_{1-y}Mn_y)PO_4$, we recollect the physical mechanism that is responsible for the two-phase region in Li_xFePO_4.[18] Both the e^--h^+ and the Li^+-V interactions by themselves are of the ordering type and do not promote phase separation, but in Li_xFePO_4 the e^--Li^+ interaction is unusually strong due to the localized Fe^{2+}/Fe^{3+} states. As this interaction dominates, Li^+ strongly attracts Fe^{2+} which in turn attracts more Li^+, leading to a two-phase state. The Fe^{2+}-Li^+ (or Fe^{3+}-V) interaction is strong and favorable enough to overcome the Li^+-Li^+ (V-V) and Fe^{2+}-Fe^{2+} (Fe^{3+}-Fe^{3+}) repulsion when all Li is brought together. This allows us to understand the trends observed in this paper. It is important to realize that in a mixed cation system such as $Li_x(Fe_{1-y}Mn_y)PO_4$, the plateau voltages are not between fully lithiated (β) and delithiated (α) states, but between α and the SS phase (for Mn^{3+}/Mn^{2+}) and between SS and β (for Fe^{3+}/Fe^{2+}). As the Fe sites are diluted by Mn, the driving force for phase separation is decreased. In the SS where Fe is largely 3+ and most Mn is 2+, some Li^+ will have Mn^{2+} neighbors, and some will have Fe^{3+} neighbors. This unfavorable interaction raises the energy of the end member of each two-phase region and lowers the transition temperature to form solid solution as observed in Fig. 4. One can also make a mean-field argument to understand the tendency toward solid solution. In $Li_y(Fe_{1-y}Mn_y)PO_4$ the Fe^{3+}-V pairs that form are diluted by Mn^{2+}-Li^+ pairs, and hence their effective interaction energy (which is attractive) is diluted, leading to a lower transition temperature. The effect of random bond disorder in lattice models has been well studied in model systems and has been shown to transform first-order transitions into second-order ones and ultimately into glassy disordered states in agreement with our results.[31–34] The disorder in the low-T single phase which we find between the two miscibility gaps for $y \approx x$ in $Li_x(Fe_{1-y}Mn_y)PO_4$ should be thought thereby as a glassy state rather than a high-T solid solution.

B. Increasing transition voltage

The variation in voltage of each redox couple with Mn/Fe concentration can be understood by considering the energy of the intermediate solid solution phase. The voltage in a two-phase reaction from $\alpha \rightarrow \beta$ is related to the energy of the two phases,[35]

$$\phi = -\left[\frac{E_{\mathrm{Li}_{x_\beta}(\mathrm{Fe,Mn})\mathrm{PO}_4} - E_{\mathrm{Li}_{x_\alpha}(\mathrm{Fe,Mn})\mathrm{PO}_4} - (x_\beta - x_\alpha)E_{\mathrm{Li}}}{x_\beta - x_\alpha}\right]. \tag{3}$$

For the sake of argument, we neglect the small solubility in the fully lithiated and delithiated phase so that the plateau voltages for Mn and Fe are the following:

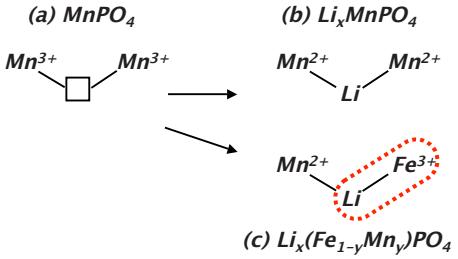

FIG. 9. (Color online) Schematic of Li site and nearest-neighbor transition-metal interactions before and after lithiation for the case of Li_xMnPO_4 compared to $Li_x(Fe_{1-y}Mn_y)PO_4$.

$$\phi_{\mathrm{Mn}} \approx -\left[\frac{E_{\mathrm{Li}_y(\mathrm{Fe}_{1-y}\mathrm{Mn}_y)\mathrm{PO}_4} - E_{(\mathrm{Fe}_{1-y}\mathrm{Mn}_y)\mathrm{PO}_4} - yE_{\mathrm{Li}}}{y}\right], \tag{4}$$

$$\phi_{\mathrm{Fe}} \approx -\left[\frac{E_{\mathrm{Li}(\mathrm{Fe}_{1-y}\mathrm{Mn}_y)\mathrm{PO}_4} - E_{\mathrm{Li}_y(\mathrm{Fe}_{1-y}\mathrm{Mn}_y)\mathrm{PO}_4} - (1-y)E_{\mathrm{Li}}}{1-y}\right]. \tag{5}$$

Consider, for example, the Mn redox voltage. In the delithiated state, all lithium vacancies are surrounded by hole states (Mn^{3+} or Fe^{3+}) just as in pure $MnPO_4$ as drawn schematically in Fig. 9. Lithiation of pure $MnPO_4$ [labeled as (a) in Fig. 9] leads to a state [$LiMnPO_4$ denoted as (b) in Fig. 9], where all Li^+ are surrounded by electron states (Mn^{2+}). This is different in the case of $Li_x(Fe_{1-y}Mn_y)PO_4$. Lithiation on the Mn plateau leads to the intermediate phase [$\approx Li_y(Fe_{1-y}Mn_y)PO_4$ labeled as (c) in Fig. 9] where Li^+ will be surrounded by some Mn^{2+} *and* some Fe^{3+}. The unfavorable Li^+-Fe^{3+} interaction (denoted by the dashed line in Fig. 9) leads to a higher average energy per Li inserted than in the pure case, hence a lower voltage. This is shown in more detail in the Appendix. Hence, it is the increased energy of the intermediate disordered state which decreases the voltage of the high redox couple (Mn) and increases the energy of the low redox couple (Fe).

C. Reduced polarization

The trend observed in Fig. 8, that the polarization of the Fe^{3+}/Fe^{2+} transition reduces as Mn substitution increases, and vice versa for the Mn^{3+}/Mn^{2+} transition, can be understood considering the composition difference between phases. Reduced polarization implies a reduced activation barrier to phase transition. At fixed temperature, the concentration difference (of Li) in the two-phase region between $Fe_{1-y}Mn_yPO_4$ (α) and $Li_yFe_{1-y}Mn_yPO_4$ (SS) monotonically decreases as the Mn composition y is increased. Similarly, the concentration difference in the two-phase region between $Li_yFe_{1-y}Mn_yPO_4$ (SS) and $LiFe_{1-y}Mn_yPO_4$ (β) monotonically increases with increasing y. For the Fe^{3+}/Fe^{2+} transition, systems with increased y must undergo less extreme fluctuations in Li concentration, so a higher number of MC moves are accepted at lower overpotential. For the Mn^{3+}/Mn^{2+} transition, the same occurs as y is decreased. Hence, the decrease in plateau voltage polarization is a fairly straightforward consequence of a reduction in the composi-

tion difference between the initial and final state along the first-order phase transition. We should point out that the polarization captured by a Monte Carlo simulation is only part of the polarization in a real electrode. Contributions from electronic resistance, surface charge transfer, strain accommodation, or interface velocity limitations cannot be modeled with our approach.

V. CONCLUSIONS

In this work, we present a framework based on first-principles calculation to model the phase behavior and electrochemical trends of mixed olivine systems, with specific emphasis on $Li_x(Fe_{1-y}Mn_y)PO_4$. Monte Carlo simulations using a Hamiltonian based on a modified coupled cluster expansion parametrized from GGA+*U ab initio* calculations of Li_xFePO_4 were used to determine the phase diagram, voltage curves, and solubility limits of $Li_x(Fe_{1-y}Mn_y)PO_4$ with significant experimental agreement. Also, experimental trends in the transition voltage and polarization are mirrored in the calculations.

Given the efficacy of the model used in this work, several insights regarding the origin of the phase behavior and electrochemical trends observed in $Li_x(Fe_{1-y}Mn_y)PO_4$ can be made. The formation of the intermediate single-phase region (SS) centered at $Li_y(Fe_{1-y}Mn_y)PO_4$ and the lowered transition temperature to form solid solution are the result of the dilution of phase-separating interactions. The attractive interaction between Mn^{2+} and Li^+ is diluted by Fe^{3+} in the SS and vice versa. Similarly, the observed changes in plateau voltages can be explained by the change in energy of the intermediate solid solution. Due to the unfavorable Li^+ coordination, the Fe^{3+} and Mn^{2+} states in the SS have higher energy than in their pure $FePO_4$ or $LiMnPO_4$ phases leading to higher and lower plateau voltages for Fe^{3+}/Fe^{2+} and Mn^{3+}/Mn^{2+}, respectively. While we have focused on the $Li_x(Fe_{1-y}Mn_y)PO_4$ system, our model to explain the variation in redox plateau voltage is likely valid for other transition-metal combinations as well, as all will have SS phases with unfavorable Li^+-M^{3+} (or V-M^{2+}) pairs separating the voltage plateaus. The trends in polarization arise as a result of the composition difference in Li between the intermediate solid solution and end-member phases.

ACKNOWLEDGMENTS

This work was supported by the U.S. Department of Energy under Contract No. DE-FG02-96ER45571, the NSF-MRSEC program under Contracts No. DMR-02-13282 and No. DMR-08-19762, and the BATT program under Contract No. DE-AC02-05CH11231 (Subcontract No. PO6806960).

APPENDIX

Neglecting triplet interactions and the small solubility in the fully lithiated and delithiated phases, the shift in the transition voltage of the Mn^{3+}/Mn^{2+} and Fe^{3+}/Fe^{2+} redox couples is shown to be independent of the point energies (J_{Fe} and J_{Mn}) and depends entirely on the Mn content y and the difference in the pair interaction energies between the completely delithiated/lithiated phase and the intermediate phase $Li_y(Fe_{1-y}Mn_y)PO_4$.

Subtracting Eq. (3) from Eq. (4) yields $\Delta\phi_{Mn}$,

$$\Delta\phi_{Mn} \approx \frac{-(E_{Li_y(Fe_{1-y}Mn_y)PO_4} - E_{(Fe_{1-y}Mn_y)PO_4})}{y} + E_{LiMnPO_4} - E_{MnPO_4}. \quad \text{(A1)}$$

Substituting Eqs. (1) and (2) into Eq. (A1), where *PI* denotes the pair interaction energies,

$$\Delta\phi_{Mn} \approx \frac{-\{[J_o - J_{Fe}(1-y) + J_{Mn}y + PI_{Li_y(Fe_{1-y}Mn_y)PO_4}] - [J_o - J_{Fe}(1-y) - J_{Mn}y + PI_{(Fe_{1-y}Mn_y)PO_4}]\}}{y} + 2J_{Mn}$$

$$= \frac{PI_{Fe_{1-y}Mn_yPO_4} - PI_{Li_yFe_{1-y}Mn_yPO_4}}{y}. \quad \text{(A2)}$$

It should be noted that $PI_{Fe_{1-y}Mn_yPO_4} = PI_{LiMnPO_4} = PI_{MnPO_4}$ since all represent states where either all Li and *e* sites are occupied, or all are unoccupied, hence equivalent pair interactions. Because of unfavorable Li^+-Fe^{3+} interactions, $PI_{Li_yFe_{1-y}Mn_yPO_4} > PI_{Fe_{1-y}Mn_yPO_4}$, which explains the negative shift in the Mn^{3+}/Mn^{2+} transition voltage in $Li_x(Fe_{1-y}Mn_y)PO_4$. A similar line of reasoning can be used to explain the positive shift in the Fe^{3+}/Fe^{2+} transition voltage in $Li_x(Fe_{1-y}Mn_y)PO_4$.

[1] A. Yamada, Y. Kudo, and K. Y. Liu, J. Electrochem. Soc. **148**, A1153 (2001).

[2] A. Yamada, Y. Takei, H. Koizumi, N. Sonoyama, R. Kanno, K. Itoh, M. Yonemura, and T. Kamiyama, Chem. Mater. **18**, 804 (2006).

[3] A. Yamada, Y. Kudo, and K. Y. Liu, J. Electrochem. Soc. **148**, A747 (2001).

[4] J. Yao, S. Bewlay, K. Konstantionv, V. A. Drozd, R. S. Liu, X. L. Wang, H. K. Liu, and G. X. Wang, J. Alloys Compd. **425**, 362 (2006).

[5] C. A. Burba and R. Frech, J. Power Sources **172**, 870 (2007).
[6] G. H. Li, H. Azuma, and M. Tohda, J. Electrochem. Soc. **149**, A743 (2002).
[7] G. H. Li, Y. Kudo, K. Y. Liu, H. Azuma, and M. Tohda, J. Electrochem. Soc. **149**, A1414 (2002).
[8] J. Molenda, W. Ojczyk, K. Swierczek, W. Zajac, F. Krok, J. Dygas, and R. S. Liu, Solid State Ionics **177**, 2617 (2006).
[9] T. Nakamura, K. Sakumoto, M. Okamoto, S. Seki, Y. Kobayashi, T. Takeuchi, M. Tabuchi, and Y. Yamada, J. Power Sources **174**, 435 (2007).
[10] T. Nakamura, K. Sakumoto, S. Seki, Y. Kobayashi, M. Tabuchi, and Y. Yamada, J. Electrochem. Soc. **154**, A1118 (2007).
[11] Y. J. Shin, J. K. Kim, G. Cheruvally, J. H. Ahn, and K. W. Kim, J. Phys. Chem. Solids **69**, 1253 (2008).
[12] D. Y. Wang, Z. X. Wang, X. J. Huang, and L. Q. Chen, J. Power Sources **146**, 580 (2005).
[13] X. J. Wang, X. Q. Yu, H. Li, X. Q. Yang, J. McBreen, and X. J. Huang, Electrochem. Commun. **10**, 1347 (2008).
[14] J. J. Chen, M. J. Vacchio, S. J. Wang, N. Chernova, P. Y. Zavalij, and M. S. Whittingham, Solid State Ionics **178**, 1676 (2008).
[15] J. Chen, S. Wang, and M. S. Whittingham, J. Power Sources **174**, 442 (2007).
[16] F. Zhou, M. Cococcioni, K. Kang, and G. Ceder, Electrochem. Commun. **6**, 1144 (2004).
[17] A. Yamada, H. Koizumi, N. Sonoyama, and R. Kanno, Electrochem. Solid-State Lett. **8**, A409 (2005).
[18] F. Zhou, T. Maxisch, and G. Ceder, Phys. Rev. Lett. **97**, 155704 (2006).
[19] C. Delacourt, P. Poizot, J. M. Tarascon, and C. Masquelier, Nature Mater. **4**, 254 (2005).
[20] J. L. Dodd, R. Yazami, and B. Fultz, Electrochem. Solid-State Lett. **9**, A151 (2006).
[21] D. Morgan, A. Van der Ven, and G. Ceder, Electrochem. Solid-State Lett. **7**, A30 (2004).
[22] S. Nishimura, G. Kobayashi, K. Ohoyama, R. Kanno, M. Yashima, and A. Yamada, Nature Mater. **7**, 707 (2008).
[23] M. S. Islam, D. J. Driscoll, C. A. J. Fisher, and P. R. Slater, Chem. Mater. **17**, 5085 (2005).
[24] C. Delmas, M. Maccario, L. Croguennec, F. Le Cras, and F. Weill, Nature Mater. **7**, 665 (2008).
[25] P. D. Tepesch, G. D. Garbulsky, and G. Ceder, Phys. Rev. Lett. **74**, 2272 (1995).
[26] A. K. Padhi, K. S. Nanjundaswamy, and J. B. Goodenough, J. Electrochem. Soc. **144**, 1188 (1997).
[27] G. H. Li, H. Azuma, and M. Tohda, Electrochem. Solid-State Lett. **5**, A135 (2002).
[28] D. P. Landau and K. Binder, *A Guide to Monte Carlo Simulations in Statistical Physics* (Cambridge University Press, Cambridge, UK, 2005).
[29] T. Nakamura, Y. Miwa, M. Tabuchi, and Y. Yamada, J. Electrochem. Soc. **153**, A1108 (2006).
[30] M. Yonemura, A. Yamada, Y. Takei, N. Sonoyama, and R. Kanno, J. Electrochem. Soc. **151**, A1352 (2004).
[31] A. Nihat Berker, Physica A **194**, 72 (1993).
[32] K. Hui and A. N. Berker, Phys. Rev. Lett. **62**, 2507 (1989).
[33] M. Aizenman and J. Wehr, Phys. Rev. Lett. **62**, 2503 (1989).
[34] A. N. Berker, J. Appl. Phys. **70**, 5941 (1991).
[35] G. Ceder, M. K. Aydinol, and A. F. Kohan, Comput. Mater. Sci. **8**, 161 (1997).